

# Thermoelectric Transport Properties in Disordered Systems Near the Anderson Transition

C. Villagonzalo<sup>a</sup>, R. A. Römer, and M. Schreiber

Institut für Physik, Technische Universität, D-09107 Chemnitz, Germany

Received: *Revision* : 1.10

**Abstract.** We study the thermoelectric transport properties in the three-dimensional Anderson model of localization near the metal-insulator transition (MIT). In particular, we investigate the dependence of the thermoelectric power  $S$ , the thermal conductivity  $K$ , and the Lorenz number  $L_0$  on temperature  $T$ . We first calculate the  $T$  dependence of the chemical potential  $\mu$  from the number density  $n$  of electrons at the MIT using an averaged density of states obtained by diagonalization. Without any additional approximation, we determine from  $\mu(T)$  the behavior of  $S$ ,  $K$  and  $L_0$  at low  $T$  as the MIT is approached. We find that  $\sigma$  and  $K$  decrease to zero at the MIT as  $T \rightarrow 0$  and show that  $S$  does not diverge. Both  $S$  and  $L_0$  become temperature independent at the MIT and depend only on the critical behavior of the conductivity.

**PACS.** 61.43.-j Disordered solids – 71.30.+h Metal-insulator transitions & other electronic transitions – 72.15.Cz Electrical and thermal conduction in amorphous & liquid metals & alloys

## 1 Introduction

The Anderson-type metal-insulator transition (MIT) has been the subject of investigation for decades since Anderson formulated the problem in 1958 [1]. He proposed that increasing the strength of a random potential in a three-dimensional (3D) lattice may cause an “absence of diffusion” for the electrons. Today, it is widely accepted that near this exclusively-disorder-induced MIT the d. c. conductivity  $\sigma$  behaves as  $|E - E_c|^\nu$ , where  $E_c$  is the critical energy or the mobility edge at which the MIT occurs, and  $\nu$  is a universal critical exponent [2]. Numerical studies based on the Anderson Hamiltonian of localization have supported this scenario with much evidence [2, 3, 4, 5, 6]. In measurements of  $\sigma$  near the MIT in semiconductors and amorphous alloys this behavior was also observed with varying values of  $\nu$  ranging from 0.5–1.3 [7, 8, 9]. It is currently believed that these different exponents are caused by interactions in the system [10]. Indeed, an MIT may be induced not only by disorder but also by interactions such as electron-electron and electron-phonon interactions, among others [11]. Nevertheless, the experimental confirmation of the critical behavior of  $\sigma$  allows the use of the Anderson model in order to describe the transition between the insulating and the metallic states in disordered systems.

Besides for the conductivity  $\sigma$ , experimental investigations can also be done for thermoelectric transport properties such as the thermoelectric power  $S$  [8, 12, 13], the thermal conductivity  $K$  and the Lorenz number  $L_0$ . The

behavior of these quantities at low temperature  $T$  in disordered systems close to the MIT has so far not been satisfactorily explained. In particular, some authors have argued that  $S$  diverges [12, 14] or that it remains constant [15, 16] as the MIT is approached from the metallic side. In addition,  $|S|$  at the MIT has been predicted [16] to be of the order of  $\sim 200 \mu\text{V/K}$ . On the other hand, measurements of  $S$  close to the MIT conducted on semiconductors for  $T \leq 1 \text{ K}$  [13] and on amorphous alloys in the range  $5 \text{ K} \leq T \leq 350 \text{ K}$  [8] yield values of the order of  $0.1\text{--}1 \mu\text{V/K}$ . They also showed that  $S$  can either be negative or positive depending on the donor concentration in semiconductors or the chemical composition of the alloy. The large difference between the theoretical and experimental values is still not resolved.

The objective of this paper is to study the behavior of the thermoelectric transport properties for the *Anderson model* of localization in disordered systems near the MIT at low  $T$ . We clarify the above mentioned difference in the theoretical calculations for  $S$ , by showing that the radius of convergence for the Sommerfeld expansion used in Refs. [14, 15] is zero at the MIT. We show that  $S$  is a finite constant at the MIT as argued in Refs. [15, 16]. Besides for  $S$ , we also compute the  $T$  dependence for  $\sigma$ ,  $K$ , and  $L_0$ . Our approach is neither restricted to a low- or high- $T$  expansion as in Refs. [14, 15], nor confined to the critical regime as in Ref. [16].

We shall first introduce the model in Sec. 2. Then in Secs. 3 and 4 we review the thermoelectric transport properties in the framework of linear response and the present formulations in calculating them. In Sec. 5 we shall show how to calculate the  $T$  dependence of these properties.

<sup>a</sup> e-mail: villagonzalo@physik.tu-chemnitz.de

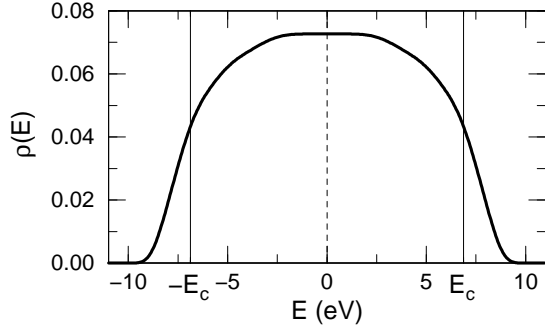


**Fig. 1.** The density of states of a 3D Anderson model, averaged over many disorder realizations with  $W = 12$ . The solid vertical lines at  $-E_c$  and  $E_c$  denote the mobility edges.

Results of these calculations are then presented in Sec. 6. Lastly, in Sec. 7 we discuss the relevance of our study to the experiments.

## 2 The Anderson Model of Localization

The Anderson model [1] is described by the Hamiltonian

$$H = \sum_i \epsilon_i |i\rangle\langle i| + \sum_{i \neq j} t_{ij} |i\rangle\langle j| \quad (1)$$

where  $\epsilon_i$  is the potential energy at the site  $i$  of a regular cubic lattice and is assumed to be randomly distributed in the range  $[-W/2, W/2]$  throughout this work. The hopping parameters  $t_{ij}$  are restricted to nearest neighbors. For this system, at strong enough disorder and in the absence of a magnetic field, the one-particle wavefunctions become exponentially localized at  $T = 0$  and  $\sigma$  vanishes [2]. Illustrating this, we refer to Fig. 1 where we show the density of states  $\rho(E)$  obtained by diagonalizing the Hamiltonian (1) with the Lanczos method as in Ref. [17,18]. The states in the band tails with energy  $|E| > E_c$  are localized within finite regions of space in the system at  $T = 0$  [2]. When the Fermi energy  $E_F$  is within these tails at  $T = 0$  the system is insulating. Otherwise, if  $|E_F| < E_c$  the system is metallic. The critical behavior of  $\sigma$  is given by

$$\sigma(E) = \begin{cases} \sigma_0 \left| 1 - \frac{E}{E_c} \right|^\nu, & |E| \leq E_c, \\ 0, & |E| > E_c, \end{cases} \quad (2)$$

where  $\sigma_0$  is a constant and  $\nu$  is the conductivity exponent [2]. Thus,  $E_c$  is called the mobility edge since it separates localized from extended states. At the critical disorder  $W_c = 16.5$ , the mobility edge occurs at  $E_c = 0$ , all states with  $|E| > 0$  are localized [3,4] and states with  $E = 0$  are multifractal [3,17]. The value of  $\nu$  has been computed from the non-linear sigma-model [19], transfer-matrix methods [2,6], Green functions methods [2], and energy-level statistics [5,20]. Here we have chosen  $\nu = 1.3$ , which is in agreement with experimental results in Si:P [9] and the numerical data of Ref. [5]. More recent numerical results [2,6], computed with higher accuracy, suggest

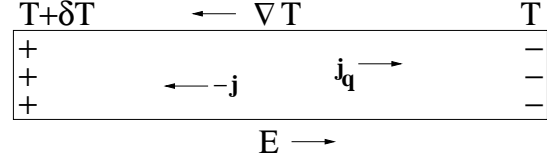


**Fig. 2.** In an open circuit, a temperature gradient  $\nabla T$  induces an electric field  $\mathbf{E}$  in the opposite direction which opposes the thermal flow of electrons.

that  $\nu = 1.5 \pm 0.1$ . As we shall show later, this difference only slightly modifies our results. We emphasize that the Hamiltonian (1) only incorporates the electronic degrees of freedom of a disordered system and further excitations such as lattice vibrations are not included.

For comparison with the experimental results, we measure  $\sigma$  in Eq. (2) in units of  $\Omega^{-1}\text{cm}^{-1}$ . We fix the energy scale by setting  $t_{ij} = 1$  eV. Hence the band width of Fig. 1 is comparable to the band width of amorphous alloys [21]. Furthermore, the experimental investigations of the thermoelectric power  $S$  in amorphous alloys [8] have been done at high electron filling [22] and thus we will mostly concentrate on the MIT at  $E_c$ .

## 3 Linear Thermoelectric Effects

### 3.1 Definition of the Transport Properties

Thermoelectric effects in a system are due mainly to the presence of a temperature gradient  $\nabla T$  and an electric field  $\mathbf{E}$  [23]. We recall that in the absence of  $\nabla T$  with  $\mathbf{E} \neq 0$ , the electric current density  $\langle \mathbf{j} \rangle$  flowing at a point in a conductor is directly proportional to  $\mathbf{E}$ ,

$$\langle \mathbf{j} \rangle = \sigma \mathbf{E}. \quad (3)$$

By applying a finite gradient  $\nabla T$  in an open circuit, electrons, the thermal conductors, would flow towards the low- $T$  end as shown in Fig. 2. This causes a build-up of negative charges at the low- $T$  end and a depletion of negative charges at the high- $T$  end. Consequently, this sets up an electric field  $\mathbf{E}$  which opposes the thermal flow of electrons. For small  $\nabla T$ , it is given as

$$\mathbf{E} = S \nabla T. \quad (4)$$

This equation defines the *thermopower*  $S$ . In the Sommerfeld free electron model of metals,  $S$  is found to be directly proportional to  $-T$  [23]. Note that the negative sign is brought about by the charge of the thermal conductors. For small  $\nabla T$ , the flow of heat in a system is proportional to  $\nabla T$ . Fourier's Law gives this as

$$\langle \mathbf{j}_q \rangle = K(-\nabla T) \quad (5)$$

where  $\langle \mathbf{j}_q \rangle$  is the heat current density and  $K$  is the thermal conductivity [23]. At low  $T$ , the phonon contribution to  $\sigma$  and  $K$  becomes negligible compared to the electronic part [23]. As  $T \rightarrow 0$ ,  $\sigma$  approaches a constant and  $K$  becomes linear in  $T$ . One can then verify the empirical law

of Wiedemann and Franz which says that the ratio of  $K$  and  $\sigma$  is directly proportional to  $T$  [24,25]. The proportionality coefficient is known as the Lorenz number  $L_0$ ,

$$L_0 = \frac{e^2}{k_B^2} \frac{K}{\sigma T} \quad (6)$$

where  $e$  is the electron charge and  $k_B$  is the Boltzmann constant. For metals, it takes the universal value  $\pi^2/3$  [23, 25]. Strictly speaking, the law of Wiedemann and Franz is valid at very low  $T$  ( $\lesssim 10$  K) and at high (room)  $T$ . This is because in these regions the electrons are scattered elastically. At  $T \sim 10 - 100$  K deviations from the law are observed which imply that  $K/\sigma T$  depends on  $T$ .

In summary, Eqs. (3)-(6) express the phenomenological description of the transport properties.

### 3.2 The Equations of Linear Response

A more compact and general way of looking at these thermoelectric “forces” and effects is as follows: the responses of a system to  $\mathbf{E}$  and  $\nabla T$  up to linear order [26] are

$$\langle \mathbf{j} \rangle = |e|^{-1} (|e| L_{11} \mathbf{E} - L_{12} T^{-1} \nabla T) \quad (7)$$

and

$$\langle \mathbf{j}_q \rangle = |e|^{-2} (|e| L_{21} \mathbf{E} - L_{22} T^{-1} \nabla T). \quad (8)$$

The kinetic coefficients  $L_{ij}$  are the keys to calculating the transport properties theoretically. Using Ohm’s law (3) in Eq. (7), we obtain

$$\sigma = L_{11}. \quad (9)$$

Also from Eq. (7),  $S$ , measured under the condition of zero electric current, is expressed as

$$S = \frac{L_{12}}{|e| T L_{11}}. \quad (10)$$

With the same condition, Eq. (8) yields

$$K = \frac{L_{22} L_{11} - L_{21} L_{12}}{|e|^2 T L_{11}}. \quad (11)$$

From Eq. (6)  $L_0$  is given as

$$L_0 = \frac{L_{22} L_{11} - L_{21} L_{12}}{(k_B T L_{11})^2}. \quad (12)$$

Therefore, we will be able to determine the transport properties once we know the coefficients  $L_{ij}$ . We note that in the absence of a magnetic field, as considered in this work, the Onsager relation  $L_{21} = L_{12}$  holds [26].

Eliminating the kinetic coefficients in Eqs. (7) and (8) in favor of the transport properties, we obtain

$$\langle \mathbf{j} \rangle = \sigma \mathbf{E} - \sigma S \nabla T \quad (13)$$

and

$$\frac{\langle \mathbf{j}_q \rangle}{T} = S \langle \mathbf{j} \rangle - \frac{K \nabla T}{T}. \quad (14)$$

Here,  $\langle \mathbf{j}_q \rangle / T$  is simply the entropy current density [26]. Hence, the thermopower is just the entropy transported per Coulomb by the flow of thermal conductors. According to the third law of thermodynamics, the entropy of a system and, thus, also  $\langle \mathbf{j}_q \rangle / T$  will go to zero as  $T \rightarrow 0$ . We can check with Eqs. (13) and (14) that this is satisfied by our calculations in the 3D Anderson model.

### 3.3 Application to the Anderson Transition

In general, the linear response coefficients  $L_{ij}$  are obtained through the Chester-Thellung-Kubo-Greenwood (CTKG) formulation [25,27]. The kinetic coefficients are expressed as

$$L_{11} = \int_{-\infty}^{\infty} A(E) \left[ -\frac{\partial f(E, \mu, T)}{\partial E} \right] dE, \quad (15)$$

$$L_{12} = - \int_{-\infty}^{\infty} A(E) [E - \mu(T)] \left[ -\frac{\partial f(E, \mu, T)}{\partial E} \right] dE, \quad (16)$$

and

$$L_{22} = \int_{-\infty}^{\infty} A(E) [E - \mu(T)]^2 \left[ -\frac{\partial f(E, \mu, T)}{\partial E} \right] dE, \quad (17)$$

where  $A(E)$  contains all the system-dependent features,  $\mu(T)$  is the chemical potential and

$$f(E, \mu, T) = 1 / \{1 + \exp([E - \mu(T)]/k_B T)\} \quad (18)$$

is the Fermi function. The CTKG approach inherently assumes that the electrons are noninteracting and that they are scattered elastically by static impurities or by lattice vibrations. A nice feature of this formulation is that all microscopic details of the system such as the dependence on the strength of the disorder enter only in  $A(E)$ . This function  $A(E)$  can be calculated in the context of the relaxation-time approximation [23]. However, an exact evaluation of  $L_{ij}$  is difficult, if not impossible, since it relies on the exact knowledge of the energy and  $T$  dependence of the relaxation time. In most instances, these are not known.

In order to incorporate the Anderson model and the MIT in the CTKG formulation, a different approach is taken: We have seen in Eq. (9) that the d.c. conductivity is just  $L_{11}$ . Thus, to take into account the MIT in this formulation, we identify  $A(E)$  with  $\sigma(E)$  given in Eq. (2). The  $L_{ij}$  in Eqs. (15)-(17) can now be easily evaluated close to the MIT without any approximation, once the  $T$  dependence of the chemical potential  $\mu$  is known. Unfortunately, this is not known for the experimental systems under consideration [7,8,9,12,13], nor for the 3D Anderson model. Thus one has to resort to approximate estimations of  $\mu$ , as we do next, or to numerical calculations, as we shall do in the next sections.

## 4 Evaluation of the Transport Coefficients

#### 4.1 Sommerfeld expansion in the metallic regime

Circumventing the computation of  $\mu(T)$ , one can use that  $-\partial f/\partial E$  is appreciable only in an energy range of the order of  $k_B T$  near  $\mu \approx E_F$ . The lowest non-zero  $T$  corrections for the  $L_{ij}$  are then accessible by the Sommerfeld expansion [23], provided that  $A(E)$  is nonsingular and slowly varying in this region. Hence, in the limit  $T \rightarrow 0$ , the transport properties are [28]

$$\sigma = A(E_F) + \frac{\pi^2}{6} (k_B T)^2 \left. \frac{d^2 A(E)}{dE^2} \right|_{E=E_F}, \quad (19)$$

$$S = -\frac{\pi^2 k_B^2 T}{3|e|A(E_F)} \left. \frac{dA(E)}{dE} \right|_{E=E_F}, \quad (20)$$

$$K = \frac{\pi^2 k_B^2 T}{3e^2} \left\{ A(E_F) - \frac{\pi^2 (k_B T)^2}{3A(E_F)} \left[ \left. \frac{dA(E)}{dE} \right]_{E=E_F}^2 \right\}, \quad (21)$$

and consequently

$$L_0 = \frac{\pi^2}{3} \left\{ 1 - \frac{\pi^2 (k_B T)^2}{3[A(E_F)]^2} \left[ \left. \frac{dA(E)}{dE} \right]_{E=E_F}^2 \right\}. \quad (22)$$

In the derivations of  $S$ ,  $K$ , and  $L_0$ , the term of order  $T^2$  in Eq. (19) has been ignored as is customary. We remark that the terms of order  $T^2$  in Eqs. (21) and (22) are usually dropped, too. In this case in the metallic regime,  $L_0$  reduces to the universal value  $\pi^2/3$  [23].

The above approach was adopted in Refs. [14] and [15] to study thermoelectric transport properties in the metallic regime close to the MIT. From Eq. (20), the authors deduce

$$S = -\frac{\nu \pi^2 k_B^2 T}{3|e|(E_F - E_c)}. \quad (23)$$

In the metallic regime, this linear  $T$  dependence of  $S$  agrees with that of the Sommerfeld model of metals [23]. However, setting  $A(E) = \sigma(E)$  at the MIT [14] in Eq. (2) is in contradiction to the basic assumption of the Sommerfeld expansion, since it is not smoothly varying at  $E_F = E_c$ . Thus identifying  $A(E) = \sigma(E)$  in Eqs. 19 - 22 is only valid in the metallic regime with  $k_B T \ll |E_c - E_F|$ .

#### 4.2 Exact calculation at $\mu(T) = E_c$

A different approach taken by Enderby and Barnes is to fix  $\mu = -E_c$  at finite  $T$  and later take the limit  $T \rightarrow 0$  [16]. Thus, again without knowing the explicit  $T$  dependence of  $\mu$ , the coefficients  $L_{ij}$  can be evaluated at the MIT. For the transport properties they obtain,

$$\sigma = \frac{\sigma_o \nu (k_B T)^\nu I_\nu}{|E_c|^\nu}, \quad (24)$$

$$S = -\frac{k_B}{|e|} \frac{\nu + 1}{\nu} \frac{I_{\nu+1}}{I_\nu}, \quad (25)$$

$$K = \frac{\sigma_o (k_B T)^{\nu+2}}{e^2 T |E_c|^\nu} \left[ (\nu + 2) I_{\nu+2} - \frac{(\nu + 1)^2 I_{\nu+1}^2}{\nu I_\nu} \right], \quad (26)$$

and

$$L_0 = \left[ \frac{(\nu + 2) I_{\nu+2}}{\nu I_\nu} - \frac{(\nu + 1)^2 I_{\nu+1}^2}{(\nu I_\nu)^2} \right]. \quad (27)$$

Here  $I_1 = \ln 2$ ,  $I_\nu = (1 - 2^{1-\nu}) \Gamma(\nu) \zeta(\nu)$  for  $\text{Re}(\nu) > 0$ ,  $\nu \neq 1$ , with  $\Gamma(\nu)$  and  $\zeta(\nu)$  the usual gamma and Riemann zeta functions. We see that at the MIT,  $S$  does not diverge nor go to zero but remains a universal constant. Its value depends only on the conductivity exponent  $\nu$ . This is in contrast to the result (23) of the Sommerfeld expansion. In addition, we find that  $\sigma \propto T^\nu$  and  $K \propto T^{\nu+1}$  as  $T \rightarrow 0$ . Hence,  $\sigma$  and  $K/T$  approach zero in the same way. This signifies that the Wiedemann and Franz law is also valid at the MIT recovering an earlier result in Ref. [29] obtained via diagrammatic methods. However, at the MIT,  $L_0$  does not approach  $\pi^2/3$  but again depends on  $\nu$ . We emphasize that Eqs. (24)-(27) are exact at  $T$  values such that  $\mu(T) - E_c = 0$  [16]. Thus the  $T$  dependence of  $\sigma$ ,  $S$ ,  $K$ , and  $L_0$  for a given electron density can only be determined if one knows the corresponding  $\mu(T)$ .

#### 4.3 High-temperature expansion

In this section, we will study the lowest-order corrections to the results obtained before with  $\mu(T) = E_c$ . We do this by expanding the Fermi function (18) for  $|E_c - \mu(T)| \ll k_B T$ . In addition, we assume  $\mu(T) \approx E_F$  for the temperature range considered. This procedure gives

$$\sigma = L_{11} = \frac{\sigma_o \nu (k_B T)^\nu}{|E_c|^\nu} \left[ I_\nu - (\nu - 1) I_{\nu-1} \frac{E_c - E_F}{k_B T} \right]. \quad (28)$$

For the thermopower, the leading-order correction can be obtained without expanding  $f(E, \mu, T)$  in  $L_{11}$  and  $L_{12}$ . This yields a constant for  $S$  at the MIT [15]. We obtain

$$S = -\frac{k_B}{|e|} \left[ \frac{\nu + 1}{\nu} \frac{I_{\nu+1}}{I_\nu} + \frac{E_c - E_F}{k_B T} \right]. \quad (29)$$

For  $K$  and  $L_0$ , we again have to use the expansion of  $f(E, \mu, T)$  as in (28) in order to get non-trivial terms. The resulting expressions are cumbersome and we thus refrain from showing them here. We remark that the basic ingredients used in the high- $T$  expansion are somewhat contradictory, namely, the expansion is valid for high  $T$  such that  $|E_c - E_F| \ll k_B T$ , whereas  $\mu(T) = E_F$  is true only for  $T = 0$ .

At present, we thus have various methods of circumventing the explicit computation of  $\mu(T)$ . However, their ranges of validity are not overlapping and it is a priori not clear whether the assumptions for  $\mu(T)$  are justified for  $S$  or any of the other transport properties close to the MIT. In order to clarify the situation, we numerically compute  $\mu(T)$  in the next section and then use the CTKG formulation to compute the thermal properties without any approximation.

## 5 The Numerical Method

In Eqs. (15)-(17), the explicit  $T$  dependence of the coefficients  $L_{ij}$  occurs in  $f(E, \mu, T)$  and  $\mu(T)$ . More precisely, knowing  $\mu(T)$ , it is straightforward to evaluate the  $L_{ij}$ . We recall that, for any set of noninteracting particles, the number density of particles  $n$  can be determined as

$$n(\mu, T) = \int_{-\infty}^{\infty} dE \rho(E) f(E, \mu, T), \quad (30)$$

where  $\rho(E)$  is again the density of energy levels (in the unit volume) as in Fig. 1. Vice versa, if we know  $n$  and  $\rho(E)$  we can solve Eq. (30) for  $\mu(T)$ . The density of states  $\rho(E)$  for the 3D Anderson model has been obtained for different disorder strengths  $W$  as outlined in Sec. 2. We determine  $\rho(E)$  with an energy resolution of at least 0.1 meV ( $\sim 1$  K). Using  $\rho(E)$ , we first numerically calculate  $n$  at  $T = 0$  for the metallic, critical and insulating regimes using the respective Fermi energies  $|E_F| < E_c$ ,  $E_F = E_c$ , and  $|E_F| > E_c$ . With  $\mu = E_F$ , we have

$$n(E_F) = \int_{-\infty}^{E_F} dE \rho(E). \quad (31)$$

Next, keeping  $n$  fixed at  $n(E_F)$ , we numerically determine  $\mu(T)$  for small  $T > 0$  such that  $|n(E_F) - n(\mu, T)|$  is zero. Then we increase  $T$  and record the respective changes in  $\mu(T)$ . Using this result in Eqs. (15)-(17) in the CTKG formulation, we compute  $L_{ij}$  by numerical integration and subsequently determine the  $T$  dependent transport properties (9)-(12).

We consider the disorders  $W = 8, 12$ , and  $14$  where we do not have large fluctuations in the density of states. These values are not too close to the critical disorder  $W_c$ , so that we could clearly observe the MIT of Eq. (2). The respective values of  $E_c$  have been calculated previously [3] to be close to 7.0, 7.5, and 8.0. Within our approach, we choose  $E_c$  to be equal to these values.

## 6 Results and Discussions

Here we show the results obtained for  $W = 12$  with  $E_c = 7.5$ . The results for  $\sigma$ ,  $K$ , and  $L_0$  are the same at  $-E_c$  and  $E_c$  since they are functions of  $L_{11}$ ,  $L_{22}$  and  $L_{12}^2$ , only. On the other hand, this is not true for  $S$ .

### 6.1 The Chemical Potential

In Fig. 3, we show how  $\mu(T)$  behaves for the 3D Anderson model at  $E_F - E_c = 0$ , and  $\pm 0.01$ . To compare results from different energy regions we plot the difference of  $\mu(T)$  from  $E_F$ . We find that  $\mu(T)$  behaves similarly in the metallic and insulating regions and at the MIT for both mobility edges at low  $T$ . In all cases we observe  $\mu(T) \propto T^2$ . Furthermore, we see that  $\mu(T)$  at  $-E_c$  equals  $-\mu(T)$  at  $E_c$ . This symmetric behavior with respect to  $E_F = \mu$  reflects

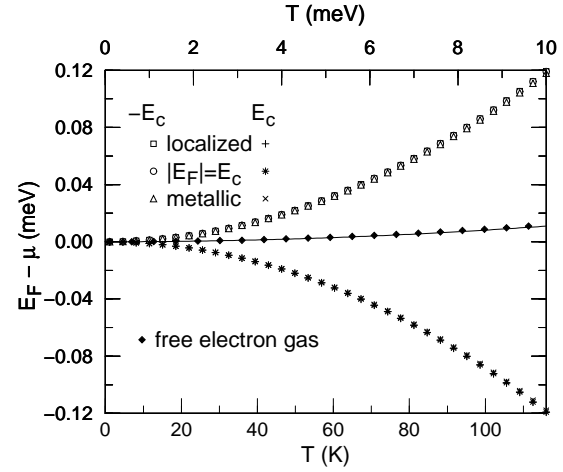


**Fig. 3.** The temperature dependence of the chemical potential  $\mu$  measured with respect to the Fermi energy near both mobility edges. Also shown is  $\mu(T)$  for a free electron gas. The solid line denotes  $\mu(T)$  of Eq. (33).

the symmetry of the density of states at  $E = 0$  as shown in Fig. 1.

For comparison and as a check to our numerics, we also compute with our method  $\mu(T)$  of a free electron gas. The density of states is [23]

$$\rho(E) = \frac{3}{2} \frac{n}{E_F} \left( \frac{E}{E_F} \right)^{1/2} \quad (32)$$

and we again use  $E_F = E_c = 7.5$ . We remark that this value of the mobility edge is in a region where  $\rho(E)$  increases with  $E$  in an analogous way as  $\rho(E)$  for the Anderson model at  $-E_c$ . Thus, as shown in Fig. 3,  $\mu(T)$  of a free electron gas is concave upwards as in the case of the Anderson model at  $-E_c$ . We also plot the result for  $\mu(T)$  obtained by the usual Sommerfeld expansion for Eq. (30),

$$E_F - \mu(T) = \frac{E_F}{3} \left( \frac{\pi k_B T}{2 E_F} \right)^2. \quad (33)$$

We see that our numerical approach is in perfect agreement with the free electron result.

### 6.2 The d.c. Conductivity

In Fig. 4 we show the  $T$  dependence of  $\sigma$ . The values of  $E_F$  we consider and the corresponding fillings  $n$  are given in Tab. 1. The conductivity at  $T = 0$  remains finite in the metallic regime with  $\sigma/\sigma_0 = |1 - E_F/E_c|^\nu$ , because  $(-\partial f/\partial E) \rightarrow \delta(E - E_F)$  in Eq. (15) as  $T \rightarrow 0$ . Correspondingly, we find  $\sigma = 0$  in the insulating regime at  $T = 0$ . In the critical regime,  $\sigma(T \rightarrow 0) \sim T^\nu$ , as derived in Ref. [16], see Eq. (24). We note that as one moves away from the critical regime towards the metallic regime one finds within the accuracy of our data that  $\sigma \sim T^2$ . We observe that in the metallic regime  $\sigma$  increases for increasing  $T$ . This is different from the behavior in a real metal where

$\sigma$  decreases with increasing  $T$ . However, as explained in Sec. 2, the behavior of  $\sigma$  in Fig. 4 is due to the absence of phonons in the present model.

We also show in Fig. 4 results of the Sommerfeld expansion (19) and the high- $T$  expansion (28) for  $\sigma$ . Paradigmatic for what is to follow we see that the radius of convergence of the Sommerfeld expansion decreases for  $E_F \rightarrow E_c$  and in fact is zero in the critical regime. On the other hand, the high- $T$  expansion is very good in the critical regime down to  $T = 0$  at  $E_c = E_F$ . The small systematic differences between our numerical results and the high- $T$  expansion for large  $T$  are due to the differences in  $\mu(T)$  and  $E_F$ . The expansion becomes worse both in the metallic and insulating regimes for larger  $T$ . All of this is in complete agreement with the discussion of the expansions in Sec. 4.

### 6.3 The Thermopower

In Fig. 5, we show the behavior of the thermopower at low  $T$  near the MIT. In the metallic regime, we find  $S \rightarrow 0$  as  $T \rightarrow 0$ . At very low  $T$ ,  $S \propto T$  as predicted by the Sommerfeld expansion (23). We see that the Sommerfeld expansion is valid for not too large values of  $T$ . But upon approaching the critical regime, the expansion becomes unreliable similar to the case of the d.c. conductivity of Sec. 6.2. This behavior persists even if we include higher order terms in the derivation of  $S$  such as the  $O(T^2)$  term of Eq. (19) as shown in Fig. 5.

Before discussing the critical regime in detail, let us turn our attention to the insulating regime. Here,  $S$  becomes very large as  $T \rightarrow 0$ . We have observed that it even appears to approach infinity. A seemingly divergent behavior in the insulating regime has also been observed for Si:P [30], where it has been attributed to the thermal activation of charge carriers from  $E_F$  to the mobility edge  $E_c$ . However, there is a simpler way of looking at this phenomenon. We refer again to the open circuit in Fig. 2. Suppose we adjust  $T$  at the cooler end such that  $\nabla T$  remains constant. As  $T \rightarrow 0$  both  $\sigma$  and  $K$  vanish in the case of insulators — for  $K$  we show this in the next section.

**Table 1.** Differences of  $E_F$  and  $n(E_F)$  with respect to the mobility edge at  $E_c = 7.5$ . The density at  $E_c$  corresponds to  $n = 97.768\%$ .

regime	$E_F - E_c$ (eV)	$n(E_F) - n(E_c)$ (%)	symbol
metallic	-0.010	-0.031	○
	-0.007	-0.022	▽
	-0.005	-0.015	□
	-0.003	-0.009	△
	-0.001	-0.003	◇
critical	0.000	0.000	●
insulating	0.001	0.003	+
	0.003	0.009	×
	0.010	0.031	*

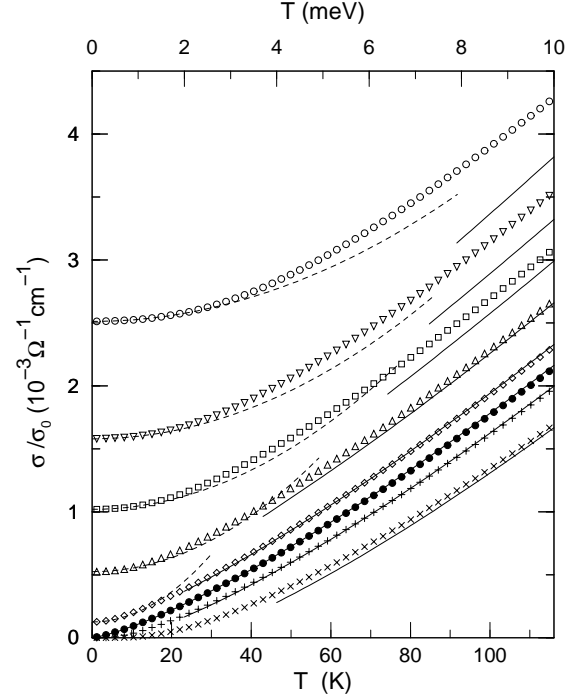


**Fig. 4.** The low temperature behavior of the d.c. conductivity  $\sigma$ . The symbols are as shown in Tab. 1. The dashed lines represent the Sommerfeld expansion result for  $\sigma(T)$  as given in Eq. (19). For all 8 choices of  $E_F - E_c$ , the corresponding high- $T$  expansion (28) is indicated by solid lines.

This implies that as  $T$  decreases it becomes increasingly difficult to move a charge from  $T$  to  $T + \delta T$ . We would need to exert a larger amount of force, and hence, a larger  $\mathbf{E}$  to do the job. From Eq. (4), this implies a larger  $S$  value.

In the critical regime, i.e., setting  $E_F = E_c$ , we observe in Fig. 5 that for  $T \rightarrow 0$  the thermopower  $S$  approaches a value of  $228.4 \mu\text{V/K}$ . This is exactly the magnitude predicted [16] by Eq. (25) for  $\nu = 1.3$ . In the inset of Fig. 5, we show that the  $T$  dependence of  $S$  is linear. The nondivergent behavior of  $S$  clearly separates the metallic from the insulating regime. Furthermore, just as for  $\sigma$ , the Sommerfeld expansion for  $S$  breaks down at  $E_F = E_c$ , i.e., the radius of convergence is zero. Thus, the divergence of Eq. (23) at  $E_F = E_c$  reflects this breakdown and is not physically relevant. On the other hand, the high- $T$  expansion [15] nicely reflects the behavior of  $S$  close to the critical regime as also shown in Fig. 5. For  $E_F = E_c$ , the high- $T$  expansion (29) assumes a constant value of  $S$  for all  $T$  due to setting  $\mu(T) = E_F$ . This is approximately valid, the differences are fairly small as shown in the inset of Fig. 5.

We stress that there is no contradiction that  $S > 0$  in our calculations whereas  $S < 0$  in Ref. [16]. In Fig. 6, we compare  $S$  in energy regions close to  $E_c$  and to  $-E_c$  [31]. Clearly, they have the same magnitude but  $S < 0$  at  $-E_c$  and  $S > 0$  at  $E_c$ . The two cases mainly differ in their number density  $n$ . At  $-E_c$  the system is at low filling with  $n = 2.26\%$  while at  $E_c$  the system is at high filling with  $n = 97.74\%$ . The sign of  $S$  implies that at low filling

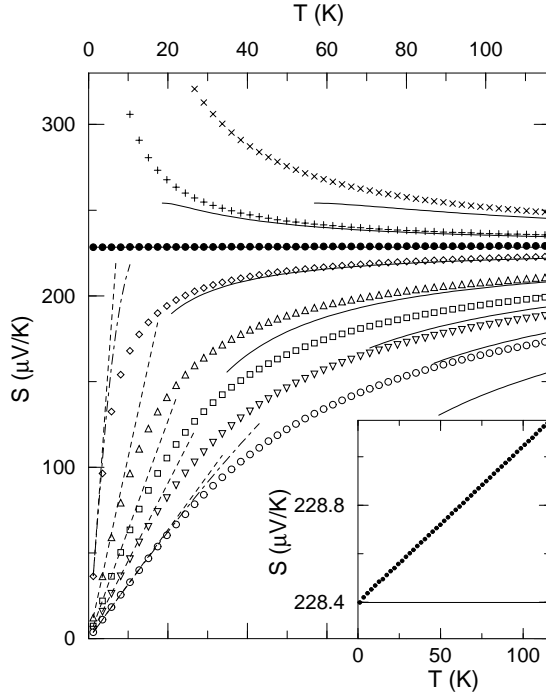


**Fig. 5.** The low temperature behavior of the thermopower  $S$ . The symbols are as shown in Tab. 1. The dashed lines represent the behavior of  $S(T)$  in the metallic regime as given in Eq. (23). The dot-dashed lines indicate  $S$ , calculated with the  $O(T^2)$  term of Eq. (19), for  $E_F - E_c = -0.01$  eV ( $\circ$ ) and  $-0.001$  eV ( $\diamond$ ). Solid lines are obtained from the high- $T$  expansion (29). The inset shows the behavior at  $E_F = E_c$  on an enlarged scale.

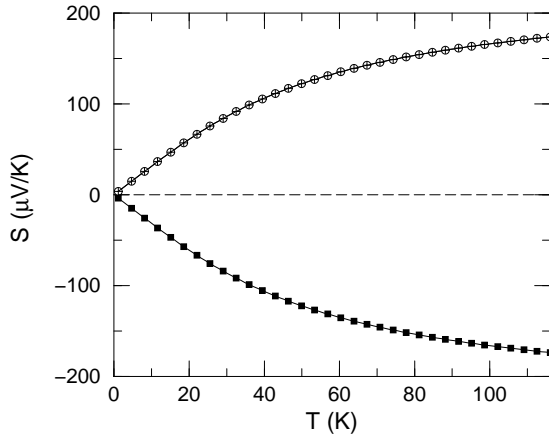


**Fig. 6.** An example that the magnitude of  $S(T)$  is the same in metallic regions close to  $-E_c$  ( $\blacksquare$ ) and  $E_c$  ( $\circ$ ). The + symbols indicate  $|S|$  for  $-E_c$  and  $|E_F - E_c| = 0.01$  eV in all cases.

the thermoelectric conduction is due to electrons and we obtain the usual picture as in Fig. 2 where the induced field  $\mathbf{E}$  is in the direction opposite to that of  $\nabla T$ . At high filling,  $S > 0$  means that  $\mathbf{E}$  is directed parallel to  $\nabla T$ . This can be interpreted as a change in charge transport from electrons to holes. We remark that this sign reversal also occurs in the insulating as well as in the critical regime.

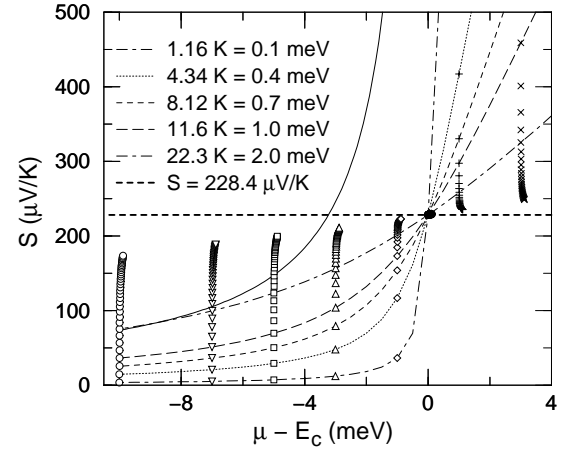


**Fig. 7.** The data of  $S$  in Fig. 5 shown as a function of  $\mu$  measured from  $E_c = 7.5$  eV. The horizontal line indicates the fixed point MIT value as given in Eq. (25). The thin dashed lines represent isotherms of  $S$  calculated using the same method as in Ref. [16]. The solid line is an isotherm of  $S$  obtained from Eq. (23) for  $T = 22.3$  K.

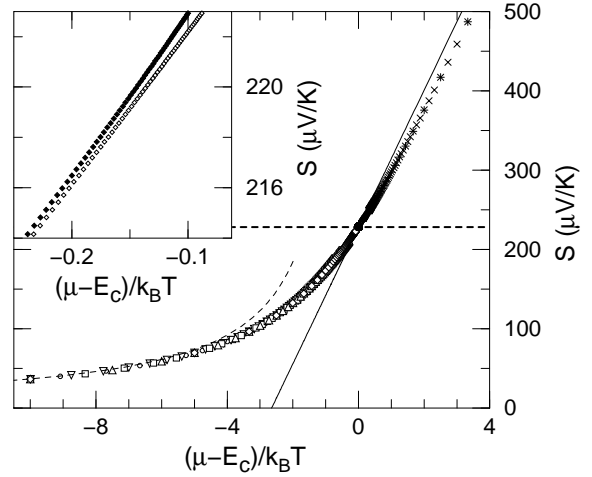


**Fig. 8.** Scaling plot of the thermopower  $S$ . The thick dashed line indicates the fixed point value at the MIT, the solid line represents the high- $T$  expansion (29), and the thin dashed line shows the Sommerfeld expansion. The inset shows the difference in the scaling when plotting  $S$  for  $E_F - E_c = -0.001$  eV as function of  $(\mu - E_c)/k_B T$  (open symbols) or  $(E_F - E_c)/k_B T$  (filled symbols).

In Fig. 7, we take the data of Fig. 5 and plot them as a function of  $\mu - E_c$ . Our data coincides with the isothermal lines which were calculated according to Ref. [16] by numerically integrating  $L_{12}$  and  $L_{11}$  for a particular  $T$  to get  $S$ . We observe that all isotherms of the insulating ( $\mu > E_c$ ) and the metallic ( $\mu < E_c$ ) regimes cross at  $\mu = E_c$  and  $S = 228.4 \mu\text{V/K}$ . Comparing with Eq. (23), we again find that the Sommerfeld expansion does not give the correct behavior of  $S$  in the critical regime.

The data presented in Fig. 7 suggest that one can scale them onto a single scaling curve. In Fig. 8, we show that

this is indeed true, when plotting  $S$  as a function of  $(\mu - E_c)/k_B T$ . We emphasize that the scaling is very good and the small width of the scaling curve is only due to the size of the symbols. The result for the high- $T$  expansion is indicated in Fig. 8 by a solid line. It is good close to the MIT. In the metallic regime, the Sommerfeld expansion correctly captures the decrease of  $S$  for large negative values of  $(\mu - E_c)/k_B T$ . We remark that a scaling with  $(E_F - E_c)/k_B T$  as predicted in Ref. [15] is approximately valid. The differences are very small as shown in the inset of Fig. 8.

#### 6.4 The Thermal Conductivity and the Lorenz Number

In Fig. 9, we show the  $T$  dependence of the thermal conductivity  $K$ . We see that  $K \rightarrow 0$  as  $T \rightarrow 0$  whether it be in the metallic or insulating regime. We note again that this simple behavior is due to the fact that our model does not incorporate phonon contributions. The  $T$  dependence of  $K$  varies whether one is in the metallic regime or in the insulating regime and how far one is from the MIT. Directly at the MIT, we find that  $K \rightarrow 0$  as  $T^{\nu+1}$  confirming the  $T$  dependence of  $K$  as given in Eq. (26). Near the localization MIT, the  $T$  dependence of  $K/T$  is thus the same as for  $\sigma$  in agreement with Ref. [29]. Again, we see that the Sommerfeld expansion (21) is reasonable only at low  $T$  in the metallic regime. As for  $\sigma$  and  $S$ , we see that the high- $T$  expansion is again fairly good in the vicinity of the critical regime.

At this point we are able to determine the behavior of the entropy in the system as  $T \rightarrow 0$ . In the metallic regime,  $S$  and  $K$  vanish as  $T \rightarrow 0$ , while in the critical and insulating regime,  $\sigma$  and  $K$  vanish as  $T \rightarrow 0$ . Applying these results to Eqs. (13) and (14) yields that for all regimes the entropy current density  $\langle \mathbf{j}_q \rangle / T$  vanishes as  $T \rightarrow 0$ . Therefore, we find that the third law of thermodynamics is satisfied for our numerical results of the 3D Anderson model.

Next, we present the Lorenz number (6) as a function of  $T$  in Fig. 10. In the metallic regime, we obtain the universal value  $\pi^2/3$  as  $T \rightarrow 0$ . Note that for a metal this value should hold up to room  $T$  [23]. However, our results for the Anderson model show a nontrivial  $T$  dependence. One might have hoped that the higher-order terms in Eq. (22) could adequately reflect the  $T$  dependence of our  $L_0$  data. However, this is not the case as shown in Fig. 10. This indicates that even if we incorporate higher order  $T$  corrections the Sommerfeld expansion will not give the right behavior of  $L_0$  near the MIT. We emphasize that the radius of convergence of Eq. (22) is even smaller than for  $\sigma$ ,  $S$  and  $K$ . Similarly, the high- $T$  expansion is also much worse than previously for  $\sigma$ ,  $S$  and  $K$ . Thus in addition to the results for the critical regime, we only show in Fig. 10 the results for nearby data sets in the insulating and metallic regimes. The  $T$  dependence of  $L_0$  is linear as shown in the inset of Fig. 10. As before for  $S$ , the high- $T$  expansion does not reproduce this. At the MIT,  $L_0 = 2.4142$ . This is again the predicted [16]  $\nu$ -dependent value as given in Eq. (27).

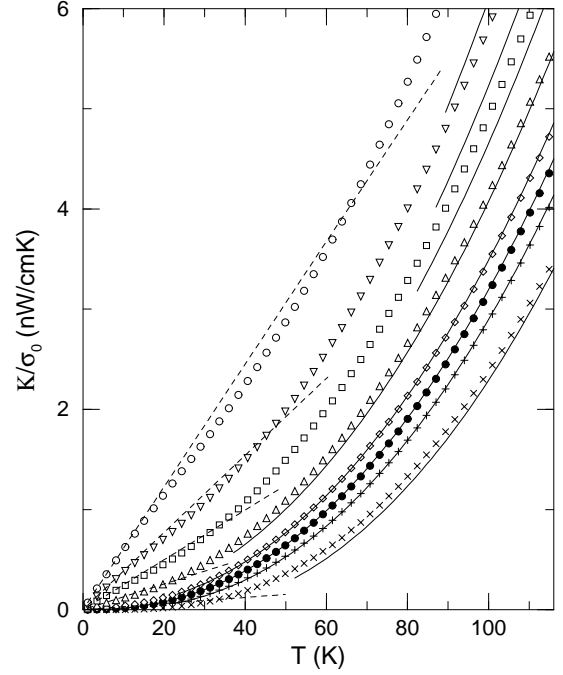


**Fig. 9.** The thermal conductivity  $K$  as a function of temperature. The symbols are as shown in Tab. 1. The dashed lines were obtained in  $O(T)$  from the Sommerfeld expansion (21) for the metallic regime. The results of the high- $T$  expansion for the 8 choices of  $E_F - E_c$  are indicated by solid lines.

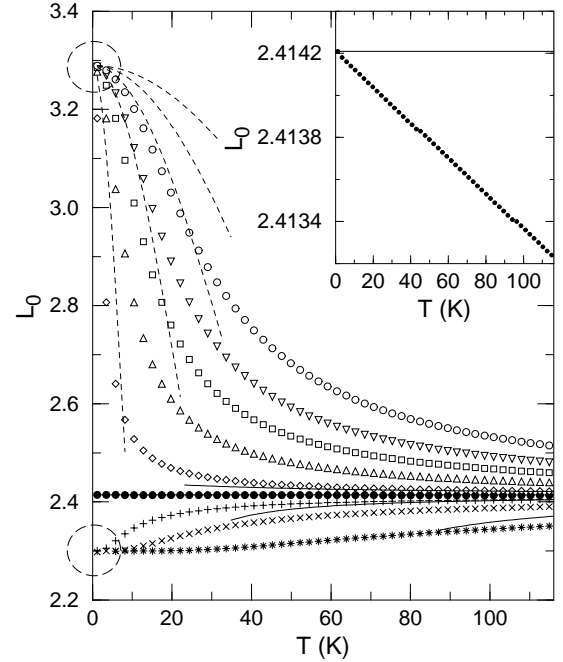


**Fig. 10.** The Lorenz number  $L_0$  as function of temperature. The symbols are as shown in Tab. 1. The dashed circles mark the values of  $L_0$  at  $T = 0$  for metallic and insulating regimes. The dashed lines were obtained from Eq. (22). The results of the high- $T$  expansion for  $E_F - E_c = 0$  eV,  $\pm 0.001$  eV and  $0.003$  eV are indicated by solid lines. The inset shows the behavior at  $E_F = E_c$  on an enlarged scale.



In the insulating regime, one can show analytically by taking the appropriate limits that  $L_0$  approaches  $\nu + 1$  as  $T \rightarrow 0$ . In agreement with this, we find that  $L_0 = 2.3$  at  $T = 0$  in Fig. 10. At first glance, it may appear surprising that a transport property in the insulating regime could be determined by a universal constant of the critical regime such as  $\nu$ . However, in the evaluation of the coefficients  $L_{ij}$ , the derivative of the Fermi function for any finite  $T$  decays exponentially and thus one will always have a non-zero overlap with the critical regime. In the evaluation of Eq. (12), this  $\nu$  dependence survives in the limit  $T \rightarrow 0$ . In real materials, we expect the relevant high-energy transfer processes to be dominated by other scattering events and thus  $L_0$  should be different. Nevertheless, for the present model, this  $\nu$  dependence holds.

### 6.5 Possible Scenarios in the Critical Regime

The results presented in Sec. 6.3 for the thermopower at the MIT show that  $S = 228.4 \mu\text{V/K}$  for  $\nu = 1.3$ . This value is 2 orders of magnitude larger than those measured near the MIT [8, 12, 13]. However, as mentioned in the introduction, the conductivity exponents found in many experiments are either close  $\nu = 0.5$  or to 1 [7] and one might hope that this difference may explain the small experimental value of  $S$ . Also, recent numerical studies of the MIT by transfer-matrix methods together with non-linear finite-size scaling find  $\nu = 1.57 \pm 0.03$  [6]. In Tab. 2 we summarize the values of  $S$  and  $L_0$  at the MIT for these conductivity exponents. We see that all  $S$  values still differ by 2 orders of magnitude from the experimental results. Furthermore, we note that our results for  $S$  and  $L_0$  are independent of the unit of energy. Even if, instead of 1 eV, we had used  $t_{ij} = 1$  meV, which is appropriate in the doped semiconductors [7, 9, 13, 30], we would still obtain the values as in Tab. 2. Thus our numerical results for the thermopower of the Anderson model at the MIT show a large discrepancy from experimental results. This may be due to our assumption of the validity of Eq. (2) for a large range of energies, or due to the absence of a true Anderson-type MIT in real materials, or due to problems in the experiments.

A different scenario for a disorder driven MIT has been proposed by Mott, who argued that the MIT from the metallic state to the insulating state is discontinuous [32].

**Table 2.** The thermopower and the Lorenz number at the MIT for a 3D Anderson model evaluated for various  $\nu$  at  $E_c = 7.5$  eV. The values for  $\nu = 0.5$  and 1 have already been shown in Ref. [16].

$\nu$	$S$ ( $\mu\text{V/K}$ )	$L_0$
0.5	163.5	1.7761
1.0	204.5	2.1721
1.3	228.4	2.4142
1.57	249.7	2.6372

Results supporting such a behavior have been found experimentally [11, 33]. According to this scenario,  $\sigma$  drops from a finite value  $\sigma_{min}$  to zero [32] for  $T = 0$  at the MIT. This minimum metallic conductivity  $\sigma_{min}$  was estimated by Mott to be

$$\sigma_{min} \simeq \frac{1}{a} \frac{e^2}{\hbar} \quad (34)$$

where  $a$  is some microscopic length of the system such as the inverse of the Fermi wave number,  $a \approx k_F^{-1}$ . As summarized in Ref. [11], experiments in non-crystalline materials seem to indicate that  $\sigma_{min} > 300 \Omega^{-1}\text{cm}^{-1}$ . Let us assume the behavior of  $\sigma(E)$  close to the MIT to be

$$\sigma(E) = \begin{cases} \sigma_{min}, & |E| \leq E_c, \\ 0, & |E| > E_c, \end{cases} \quad (35)$$

with  $\sigma_{min} = 300 \Omega^{-1}\text{cm}^{-1}$ . Using the numerical approach of Sec. 5, we obtain  $S = 119.5 \mu\text{V/K}$  at the MIT. This value is still rather large and thus the assumption of a minimum metallic conductivity as in Eq. (35) cannot explain the discrepancy from the experimental results. We remark that the order of magnitude of  $S$  is not changed appreciably, even if we add to the metallic side of Eq. (35) a term as given in Eq. (2) with  $\sigma_0$  a few hundred  $\Omega^{-1}\text{cm}^{-1}$  and  $\nu = 1$ .

Lastly, we note that the transport properties calculated for  $W = 8$  and 14 do not differ from those obtained for  $W = 12$  in both the metallic and insulating regions provided we are at temperatures  $T \lesssim 100\text{K}$ . For  $S$  and  $L_0$  at the MIT we obtain the same values as for  $W = 12$ . Again we observe that both  $S$  and  $L_0$  approach these values linearly with  $T$ , but with different slopes. Our results show that the higher the disorder strength the smaller the magnitude of the slope.

## 7 Conclusions

In this paper, we investigated the thermoelectric effects in the 3D Anderson model near the MIT. The  $T$  dependence of the transport properties is determined by  $\mu(T)$ . We were able to compute  $\mu(T)$  by numerically inverting the formula for the number density  $n(\mu, T)$  of non-interacting particles. Using the result for  $\mu(T)$ , we calculated the thermoelectric transport properties within the Chester-Thellung-Kubo-Greenwood formulation of linear response. As  $T \rightarrow 0$  in the metallic regime we verified that  $\sigma$  remains finite,  $S \rightarrow 0$ ,  $K \rightarrow 0$  and  $L_0 \rightarrow \pi^2/3$ . On the other hand, in the insulating regime,  $S \rightarrow \infty$ . This we attribute to both  $\sigma$  and  $K$  going to zero. Thus, it becomes increasingly difficult to achieve equilibrium and, hence, the system requires  $\mathbf{E} \rightarrow \infty$ . For  $L_0$ , we obtained a universal value of  $\nu + 1$  even in the insulating regime. Directly at the MIT, the thermoelectric transport properties agree with those obtained in Ref. [16]. Namely, as  $T \rightarrow 0$ , we found  $\sigma \sim T^\nu$ ,  $K \sim T^{\nu+1}$ , while  $L_0 \rightarrow \text{const.}$

The thermopower  $S$  also remains nearly constant in the critical regime and, in particular, it does not diverge at the MIT in contrast to earlier calculations using the

Sommerfeld expansion at low  $T$  [14]. Here we showed that the difference is not so much due to an order of limits problem, but rather reflects the breakdown of convergence of the Sommerfeld expansion at the MIT [15]. Our result is supported by scaling data for  $S$  at different values of  $T$  and  $E_F$  onto a single curve which is continuous across the transition. Some of the experiments [8,12] for  $S$  have been influenced by the Sommerfeld expansion such that the authors plot their results as  $S/T$ . We remark that in such a plot the signature of the MIT is hard to identify, since  $S/T$  at the MIT diverges as  $T \rightarrow 0$  solely due to the decrease in  $T$ . Our results suggest that plots as in Figs. 5 and 7 should show the MIT more clearly.

The value of  $S$  is at least two orders of magnitude larger than observed in experiments [8,12,13]. This large discrepancy may be due to the ingredients of our study, namely, we assumed that a simple power-law behavior of the conductivity  $\sigma(E)$  as in Eq. (2) was valid even for  $E \ll E_c$  and  $E \gg E_c$ . Furthermore, we assumed that it is enough to consider an averaged density of states  $\rho(E)$ . While the first assumption is of course crucial, the second assumption is of less importance as we have checked: Local fluctuations in  $\rho(E)$  will lead to fluctuations in the thermoelectric properties for finite  $T$ , but do not lead to a different  $T \rightarrow 0$  behavior:  $S$  remains finite with values as given in Tab. 2. Moreover, averaging over many samples yields a suppression of these fluctuations and a recovery of the previous behavior for finite  $T$ . In this context, we remark that — naively assuming all other parts of the derivation are unchanged — implications of many-particle interactions such as a reduced single-particle density of states at  $E_F$  [34], will only modify the  $T$  dependence of  $\mu$ . Consequently, the  $T$  dependencies of  $S$ ,  $\sigma$ ,  $K$ , and  $L_0$  may be different, but their values at the MIT remain the same.

Our results also suggest that the critical regime is very small. Namely, as the filling increases slightly from  $n = 97.74\%$  to  $97.80\%$ , the behavior of the system changes from metallic to critical and finally to insulating. Up to the best of our knowledge, such small changes in the electron concentration have not been used in the measurements of  $S$  as in Refs. [8,12,13]. We emphasize that such a fine tuning of  $n$  is not essential for measurements of  $\sigma$  as is apparent from Fig. 4.

Of course, one may also speculate [16] that these results suggest that a true Anderson-type MIT has not yet been observed in the experiments.

We thank Frank Milde for programming help and Thomas Vojta for useful and stimulating discussions. We gratefully acknowledge stimulating communications from John E. Enderby and Yoseph Imry. This work has been supported by the DFG as part of SFB393.

## References

1. P. W. Anderson, Phys. Rev. **109**, (1958) 1492.
2. See for example B. Kramer and A. MacKinnon, Rep. Prog. Phys. **56**, (1993) 1469 and references therein.

3. H. Grussbach and M. Schreiber, Phys. Rev. B **51**, (1995) 663.
4. B. Bulka, M. Schreiber and B. Kramer, Z. Phys. B - Condensed Matter **66**, (1987) 21.
5. E. Hofstetter and M. Schreiber, Phys. Rev. Lett. **73**, (1994) 3137; E. Hofstetter and M. Schreiber, Phys. Rev. B **49**, (1994) 14726.
6. K. Slevin and T. Ohtsuki, Phys. Rev. Lett. **82** (1999) 382; P. Cain, R. A. Römer, and M. Schreiber, preprint (1999).
7. Th. Zint, M. Rohde and H. Micklitz, Phys. Rev. B. **41**, (1990) 4831; U. Thomanschefsky and D. F. Holcomb, Phys. Rev. B. **45**, (1992) 13356; M. J. Hirsch, U. Thomanschefsky and D. F. Holcomb, Phys. Rev. B. **37**, (1988) 8257 and references therein.
8. C. Lauinger and F. Baumann, J. Phys.: Condens. Matter **7**, (1995) 1305.
9. H. Stupp, M. Hornung, M. Lakner, O. Madel, H. v. Löhneysen, Phys. Rev. Lett. **71**, (1993), 2634.
10. D. Belitz and T. R. Kirkpatrick, Rev. Mod. Phys. **66**, (1994) 261.
11. N. F. Mott and E. A. Davis, *Electronic Processes in Non-crystalline Materials* (Clarendon Press, Oxford, 1979).
12. G. Sherwood, M. A. Howson, and G. J. Morgan, J. Phys.: Condens. Matter **3**, (1991) 9395.
13. M. Lakner and H. v. Löhneysen, Phys. Rev. Lett. **70**, (1993) 3475.
14. C. Castellani, C. Di Castro, M. Grilli, and G. Strinati, Phys. Rev. B **37**, (1988) 6663.
15. U. Sivan and Y. Imry, Phys. Rev. B **33**, (1986) 551.
16. J. E. Enderby and A.C. Barnes, Phys. Rev. B **49**, (1994) 5062.
17. F. Milde, R. A. Römer, and M. Schreiber, Phys. Rev. B **55**, (1997) 9463.
18. F. Milde and R. A. Römer, Ann. Phys. (Leipzig) **7**, (1998) 452; U. Elsner, V. Mehrmann, F. Milde, R. A. Römer, and M. Schreiber, to be published in SIAM J. Sci. Comp., (1999).
19. F. Wegner, Z. Phys. B **44**, (1981) 9; K. Efetov, *Super-symmetry in disorder and chaos* (Cambridge Univ. Press, Cambridge, 1997).
20. E. Hofstetter, to be published in Phys. Rev. B (1999, cond-mat/9611060); I. Kh. Zharekeshev and B. Kramer, Phys. Rev. Lett. **79** (1997) 717.
21. P. Häussler, Phys. Reports **222**, (1992), 65.
22. P. Häussler, private communication.
23. N. W. Ashcroft and N. D. Mermin, *Solid State Physics* (Saunders College, New York, 1976).
24. G. Wiedemann and R. Franz, Ann. Phys. (Lpz.) (2) **89**, (1853) 497 (Pogg. Ann. Bd. **89**, p. 497.).
25. G. V. Chester and A. Thellung, Proc. Phys. Soc. **77**, (1961) 1005.
26. H. B. Callen, *Thermodynamics and an Introduction to Thermostatistics* (John Wiley & Sons, New York, 1985).
27. R. Kubo, J. Phys. Soc. Japan **12**, (1957) 570; D. A. Greenwood, Proc. Phys. Soc. **71**, (1958) 585.
28. The Sommerfeld expansion is used for integrals of the form  $\int_{-\infty}^{\infty} d\varepsilon H(\varepsilon) f(\varepsilon)$  where  $f(\varepsilon)$  is the Fermi function and  $H(\varepsilon)$  is nonsingular and not rapidly varying in a region of order  $k_B T$  near  $\varepsilon = \mu$ . The integral is expanded as follows

$$\int_{-\infty}^{\infty} d\varepsilon H(\varepsilon) f(\varepsilon) = \int_{-\infty}^{\mu} d\varepsilon H(\varepsilon) + \sum_{j=1}^{\infty} (k_B T)^{2j} a_j \left. \frac{d^{2j-1}}{d\varepsilon^{2j-1}} H(\varepsilon) \right|_{\varepsilon=\mu} \quad (36)$$

where  $a_j$  are dimensionless numbers. See Ref. [23] for more details.

29. G. Strinati and C. Castellani, Phys. Rev. B **36**, (1987) 2270.
30. X. Liu, *On the thermal properties of disordered solids at low temperatures: amorphous  $As_xSe_{1-x}$ , compacted amorphous  $SiO_2$ , and heavily doped  $Si:P$* , Ph.D. thesis, Universität Karlsruhe (Verlag Shaker, Aachen, 1995).
31. C. Villagonzalo and R. A. Römer, Ann. Phys. (Leipzig) **7**, (1998) 394.
32. N. F. Mott, Phil. Mag. **17**, (1968) 1259.
33. A. Möbius, C. Frenzel, R. Thielsch, R. Rosenbaum, C. J. Adkins, M. Schreiber, H.-D. Bauer, R. Grötzschel, V. Hoffman, T. Krieg, N. Matz, H. Vinzelberg, and M. Witcomb, preprint (1998, cond-mat/9812106).
34. A. L. Efros and B. Shklovskii, J. Phys. C **8**, (1975) L49, A. L. Efros, J. Phys. C **9**, (1976) 2021; F. Epperlein, M. Schreiber, and T. Vojta, Phys. Rev. B **56**, (1997) 5890; T. Vojta, F. Epperlein, and M. Schreiber, Phys. Rev. Lett. **81**, (1998) 1212.